Fig. 1. RPC spacers produced from photo-sensitive polyimide. Each spacer is 300 μm in diameter and 300 μm in height.

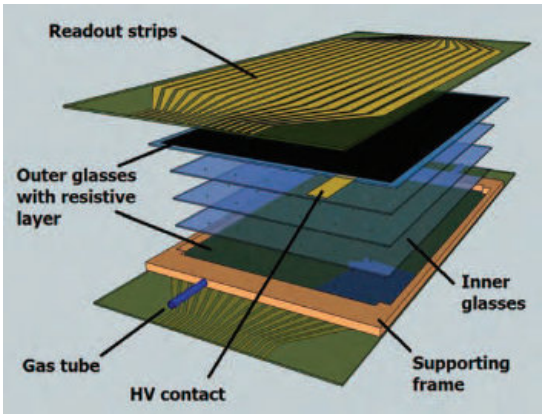

Fig. 2. Schematic of compact MRPC design for TOF-PET application.

the glass and then selectively etched in any image desirable. We have used a pattern of spacers of 300-μm diameter and 300-μm height covering the glass surface at 1-cm separation (see Fig. 1). In this way, excess mechanical support—needed to fix the fishing line—can be avoided, allowing for a very compact design that is also easier to assemble.

A schematic of an MRPC design for a PET application is shown in Fig. 2. The assembly consists of glass plates glued inside a very low-density glass-epoxy composite frame. The outmost glasses are coated with a resistive layer that allows application of a high voltage (HV). A pair of strip-readout electrodes patterned onto flexible polyimide foils are placed above the resistive layers, bringing the induced signal to the front-end electronics. The pitch between readout strips has been chosen to be 4 mm, roughly similar to the segmentation of most crystal-based PET designs.

One aspect of importance to the operation of RPCs is the value of the surface resistivity of the coating needed to apply the HV over the active area, typically measured in Ω/square. In our case, a higher resistivity is desirable since the less resistive the layer is, the more the signal produced inside the detector is spread out over the readout electrodes, resulting in a lower signal on each channel. Since we can assume that less overall charge will be induced on the electrodes when detecting 511-keV photons (only one gap fires rather than many as with charged particles), it follows that too low a resistivity will limit the detection efficiency. This point has been investigated with several types of materials. A resistivity of 1 MΩ/square, which was about the highest that could be achieved while still remaining uniform over the entire active area, was deemed suitable for our geometry. The layer is a colloidal graphite emulsion that is first applied to the glass surface and then allowed to dry, forming a thin resistive layer. Other materials that offer a resistivity higher than 1 M Ω/square are currently under investigation.

We have constructed prototype MRPC modules, having an active area of 6.5 cm × 9 cm, and tested them for gas tightness and HV stability. One example of a 4-gas-gap module is shown in Fig. 3, both before resistive coating was applied (shown left) and after the assembly was complete with the resistive coating, readout strips and front-end electronics support (shown right). Such modules use 400-μm soda-lime glass and 300-μm spacers and are only 3.2 mm thick, making it possible to stack many tens of modules into a single and compact PET camera head.

Single-gap and MRPC prototypes, similar to the ones shown in Fig. 3, were tested for their efficiency and timing properties in the laboratory. Instead of choosing to use glued modules, however, we have built RPCs using the same materials and techniques as before but housed inside larger gas chambers. These gas chambers can be disassembled easily, allowing us more flexibility in choosing the exact configuration of our RPC and MRPC prototypes. A picture of an MRPC module mounted inside such a gas chamber before it is sealed is shown in Fig. 4. In all tests, pure tetrafluoroethane gas ($C_2F_4H_2$) was circulated through the detectors at a rate of a few liters per hour.

Data acquisition was achieved with a front-end readout electronics board produced for the ALICE collaboration and

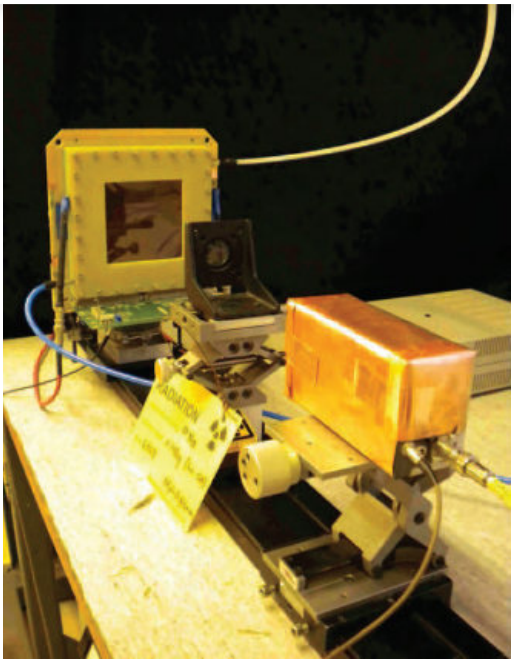

Fig. 6. The experimental setup for RPC efficiency tests with 511-keV photons.

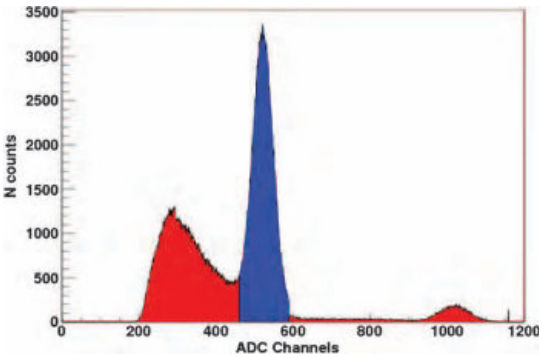

Fig. 7. An example of the selection of photoelectric events in the BGO-PMT assembly used in the RPC efficiency measurements.

pulse generator simultaneously, and were found to be limited only by the resolution of the TDC itself.

RESULTS

The efficiency of single-gap RPCs and 4-gap MRPCs, each with two different values of resistivity, has been measured as a function of the applied voltage per gap. Figure 9 shows the results for all four detector configurations. The efficiency of

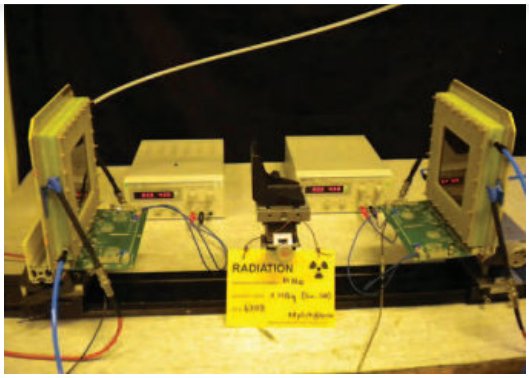

Fig. 8. The experimental setup for RPC time-of-flight measurements with 511-keV photons.

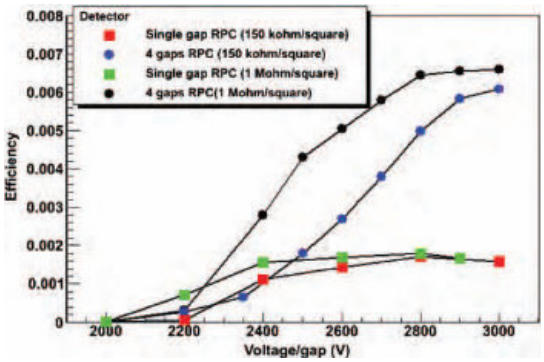

Fig. 9. Single-gap and 4-gap RPC efficiency with 511-keV gamma rays. Two values of resistivity have been used for each configuration.

single-gap RPCs was found to reach a maximum at ~ 0.18%, while for the 4-gap MRPCs the maximum was reached at ~ 0.66%. In both cases, the plateau of efficiency was reached at lower voltages for the detectors having the higher resistivity.

A preliminary result for the timing measurement for two single-gap RPC modules in coincidence is shown in Fig. 10. The result for two 4-gap MRPC modules is shown in Fig. 11. In both cases, resistive coatings of 1 MΩ/square were used. The standard deviation of the peak was 443 ps for the single-gap RPCs and 525 ps for the 4-gap MRPC modules. This translates into a single detector time resolution for 511 keV gamma rays of 310 ps and 370 ps for the single-gap and 4-gap modules, respectively.

DISCUSSION

We have developed a production technique for building compact MRPC modules that have been tested in the

large quantity. This is an important point since any RPC-PET detector must consist of many hundreds of multi-gap modules so as to achieve a sensitivity comparable to crystal-based technology.

FUNDING

This research has been supported by the Marie Curie Early Initial Training Network Fellowship of the European Community's Seventh Framework Programme under Contract No. PITN-GA-2008-215840-PARTNER.

REFERENCES

1. Fiedler F, Shakirin G, Skowron J *et al*. On the effectiveness of ion range determination from in-beam PET data. Phys Med Bio*l* 2010;**55**:1989–98.
2. Urakabe E, Kanai T, Kanazawa M *et al.* Spot scanning using radioactive C-11 beams for heavy-ion radiotherapy. *Jpn J Appl Phys* 2001;**40**:2540–8.
3. Enghardt W, Crespo P, Fiedler F *et al*. Charged hadron tumour therapy monitoring by means of PET. *Nucl Instr Meth Phys Res A* 2004;**525**:284–8.
4. Crespo P, Shakirin G, Enghardt W. On the detector arrangement for in-beam PET for hadron therapy monitoring. *Phys Med Biol* 2006;**51**:2143–63.
5. Conti M, Eriksson L, Rothfuss H *et al*. Comparison of Fast Scintillators with TOF PET Potential. *IEEE Trans Nucl Sci* 2009;**56**:926–33.

ment verification of ion therapy: implementation and experience at GSI Darmstadt and MGH Boston. *Nucl Instr Meth Phys Res A* 2008;**591**:282–6.
7. Gonzalez-Diaz D, Sharma A. Current Challenges and Perspectives in Resistive Gaseous Detectors: a manifesto from RPC 2012. *PoS* 2012;**084**:1–22.
8. An S, Jo YK, Kim JS *et al.* A 20 ps timing device – A multigap resistive plate chamber with 24 gas gaps. *Nucl Instr Meth Phys Res A* 2008;**594**:39–43.
9. Blanco A, Chepel V, Ferreira-Marques R *et al*. Perspectives for positron emission tomography with RPCs. *Nucl Instr Meth Phys Res A* 2003;**508**:88–93.
10. Couceiro M, Blanco A, Ferreira NC *et al.* RPC-PET: status and perspectives. *Nucl Instr Meth Phys Res A* 2007;**580**:915–8.
11. Ilieva N, Kozhuharov V, Lessigiarska I *et al.* Development of a Novel PET Imaging System, based on Resistive-Plate Chambers (RPC). *AIP Conf Proc* 2010;**1203**;820–5.
12. Couceiro M, Crespo P, Mendes L *et al*. Spatial resolution of human RPC-PET system. *Nucl Instr Meth Phys Res A* 2012;**661**:S156–8.
13. Abbrescia M, Alici A, An S *et al.* Performance of a six-gap MRPC built for large area coverage. *Nucl Instr Meth Phys Res A* 2008;**593**:263–8.
14. Scapparone E (on, behalf of the TOF group). The Time-of-Flight detector of the ALICE experiment. IOP Publishing. *J Phys G: Nucl Part Phys* 2007;**34**:S725–8.
15. Anghinolfi F, Jarron P, Krummenacher F *et al*. NINO: An ultrafast low-power front-end amplifier discriminator for the time-of-flight detector in the ALICE experiment. *IEEE Trans Nucl Sci* 2004;**51**:1974–8.